Kent Academic Repository
Full text document (pdf)

Citation for published version

DOI

Link to record in KAR

https://kar.kent.ac.uk/74697/

Document Version

Author's Accepted Manuscript

Valence and ionic lowest-lying electronic states of ethyl formate as studied by high-resolution vacuum ultraviolet photoabsorption, He(I) photoelectron spectroscopy and ab initio calculations

M. A. Śmiałek,[1] M. Łabuda,[2] J. Guthmuller,[2] M.-J. Hubin-Franskin,[3] J. Delwiche,[3] D. Duflot,[4] N. J. Mason,[5] S. V. Hoffmann,[6] N. C. Jones,[6] and P. Limão-Vieira[7]

[1] Department of Control and Energy Engineering, Faculty of Ocean Engineering and Ship Technology, Gdańsk University of Technology, Gabriela Narutowicza 11/12, 80-233 Gdańsk, Poland. Fax: +48583486372; Tel: +48583472614[a]

[2] Department of Theoretical Physic and Quantum Informatics, Faculty of Applied Physics and Mathematics, Gdańsk University of Technology, Gabriela Narutowicza 11/12, 80-233 Gdańsk, Poland.

[3] Département de Chimie, Université de Liège, Institut de Chimie-Bât. B6C, B-4000 Liège, Belgium.

[4] Laboratoire de Physique des Lasers, Atomes et Molécules (PhLAM), UMR CNRS 8523, Université Lille1 Sciences et Technologies, F-59655 Villeneuve d' Ascq Cedex, France.

[5] Department of Physical Sciences, The Open University, Walton Hall, Milton Keynes, MK7 6AA, United Kingdom.

[6] ISA, Department of Physics and Astronomy, Aarhus University, Ny Munkegade 120, Building 1520, DK-8000 Aarhus C, Denmark.

[7] Laboratório de Colisões Atómicas e Moleculares, CEFITEC, Departamento de Física, Faculdade de Ciências e Tecnologia, Universidade Nova de Lisboa, 2829-516 Caparica, Portugal Fax: +351212948549; Tel: +351212947859[b]

(Dated: August 22, 2014)

The highest resolution VUV photoabsorption spectrum of ethyl formate, C_2H_5OCHO, yet reported is presented over the wavelength range 115.0 to 275.5 nm (10.75 to 4.5 eV) revealing several new spectral features. Valence and Rydberg transitions and their associated vibronic series, observed in the photoabsorption spectrum, have been assigned in accordance with new ab initio calculations of the vertical excitation energies and oscillator strengths. Calculations have also been carried out to determine the ionization energies and fine structure of the lowest ionic state of ethyl formate and are compared with a newly recorded He(I) photoelectron spectrum (from 10.1 to 16.1 eV). New vibrational structure is observed in the first photoelectron band. The photoabsorption cross sections have been used to calculate the photolysis lifetime of ethyl formate in the upper stratosphere (20–50 km).

PACS numbers: Valid PACS appear here
Keywords: Suggested keywords

I. INTRODUCTION

Ethyl formate, also known as ethyl methanoate, is a volatile compound formerly used as a fumigant for grain, now restricted to use on dried fruit and processed cereal products[1]. Together with the simplest ester, methyl formate[2], ethyl formate has been detected in the interstellar space in the dust cloud, Sagittarius B2(N)[3]. Ethyl formate is also used as a model compound for combustion chemistry studies of ethyl esters, which are typical constituents of biodiesel fuels, showing their contribution in benzene and soot formation upon fuel combustion[4]. In a recent publication we reported the electronic state spectroscopy of methyl formate using high resolution vacuum ultraviolet photoabsorption, He(I) photoelectron spectroscopy and ab initio calculations, where a detailed analysis of the vibrational progressions and several Rydberg series were proposed for the first time[5].

Ethyl formate has been the subject of many theoretical and experimental studies resulting in a description of the geometry of the molecule and assignment of the observed frequencies to the vibrational modes of the molecule[6–9]. Ionization and dissociation of ethyl formate by electron impact has also been investigated[10]. Photoionization energies together with ion mass spectrometry were obtained through a He(I) ionization source[11,12], synchrotron radiation and a femtosecond laser[13]. The values obtained by other investigators are in a good agreement with the present data despite the higher resolution achieved in this study.

In this paper we present high resolution VUV photoabsorption spectra with absolute cross sections, together

[a] Electronic mail: smialek@pg.gda.pl; Also at Department of Physical Sciences, The Open University, Walton Hall, Milton Keynes, MK7 6AA, United Kingdom.

[b] Also at Department of Physical Sciences, The Open University, Walton Hall, Milton Keynes, MK7 6AA, United Kingdom.; Electronic mail: plimaovieira@fct.unl.pt

with theoretical calculations of the vertical excitation energies and oscillator strengths of the electronic transitions of ethyl formate. To our knowledge, no high resolution studies have been reported for this molecule yet. Additionally, the He(I) photoelectron spectrum was measured and analyzed in order to clarify Rydberg assignments in the VUV spectrum. These data also provide, for the first time, a vibrational resolution of the first ionic band of ethyl formate. Absolute photoabsorption cross sections are needed in modeling studies of the Earth atmosphere and radiation chemistry of aliphatic esters.

II. EXPERIMENTAL PROCEDURE

A. Ethyl formate sample

The liquid sample used both in the VUV measurements and the PES experiment was purchased from Sigma-Aldrich, with a purity of 97 %. The sample was degassed by repeated freeze–pump–thaw cycles in both sets of experiments.

B. VUV photoabsorption

The high-resolution VUV photoabsorption spectrum of ethyl formate (Fig. 1) was measured at the UV1 beam line, using the ASTRID synchrotron facility in Aarhus University, Denmark. The experimental apparatus has been described in detail previously[14]. Synchrotron radiation passes through a static gas sample and a photomultiplier is used to measure the transmitted light intensity. The incident wavelength is selected using a toroidal dispersion grating with 2000 lines/mm, providing a resolution of 0.1 nm, corresponding to 3 meV at the midpoint of the energy range studied. The minimum wavelength to which scans are performed, 115 nm (10.8 eV), is determined by the windows of the gas cell (LiF entrance and MgF_2 exit).

The sample pressure is measured using a capacitance manometer (Baratron). To ensure that the data were free of any saturation effects[15,16], the cross sections were measured over the pressure range 0.07–1.27 mbar with typical attenuations < 40 %. A background scan is recorded with the cell evacuated. Absolute photoabsorption cross sections are then obtained using the Beer–Lambert attenuation law

$$I_t = I_0 \times \exp(-n\sigma x),$$

where I_t is the radiation intensity transmitted through the gas sample, I_0 is that through the evacuated cell, n is the molecular number density of the sample gas, σ is the absolute photoabsorption cross section, and x is the absorption path length (25 cm). The accuracy of the cross section is estimated to be better than ±5 %. Only when absorption by the sample is very weak ($I_0 \approx I_t$), does

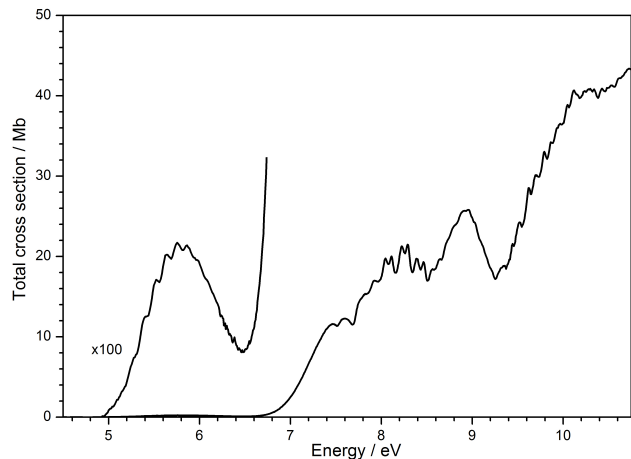the uncertainty increase as a percentage of the measured cross section.

Figure 1. High resolution photoabsorption spectrum of ethyl formate.

C. Photoelectron spectroscopy

The He(I) (21.22 eV) photoelectron spectrum of ethyl formate (Fig. 2 was measured at the Université de Liège, Belgium. The apparatus has been described in detail previously[17]. Briefly, it consists of a 180° hemispherical electrostatic analyzer with a mean radius of 5 cm. The analyzer is used in the constant pass energy mode. The incident photons are produced by a D.C. discharge in a two-stage differentially pumped lamp. The energy scale is calibrated using the $X^2\Sigma_g^+$, $v' = 0$ and $A^2\Pi_u$, $v' = 0$ peaks of N_2^+, rounded to three decimal places[18,19]. The resolution of the present spectrum is 55 meV and the accuracy of the energy scale is estimated to be ± 2 meV. The photoelectron spectrum presented in this paper is the sum of 70 individual spectra. This procedure allows us obtain a good signal-to-noise ratio while keeping the pressure in the spectrometer low ($< 5 \times 10^{-6}$ mbar), thus minimizing the occurrence of dimers.

III. COMPUTATIONAL METHODS

The ground state geometry, harmonic vibrational frequencies, and normal coordinates of the neutral singlet state (S_0) and ionic doublet state (D_0) of ethyl formate were obtained with the Gaussian 09 program[20] by means of second-order Møller-Plesset (MP2) calculations in association with the aug-cc-pVTZ basis set[21]. The ionic state was described by open-shell unrestricted calculations. The first ionization energies (IE) were computed from the energy difference between the neutral and ionic ground states. The vertical IE was calculated at the ground state geometry of the neutral compound and the
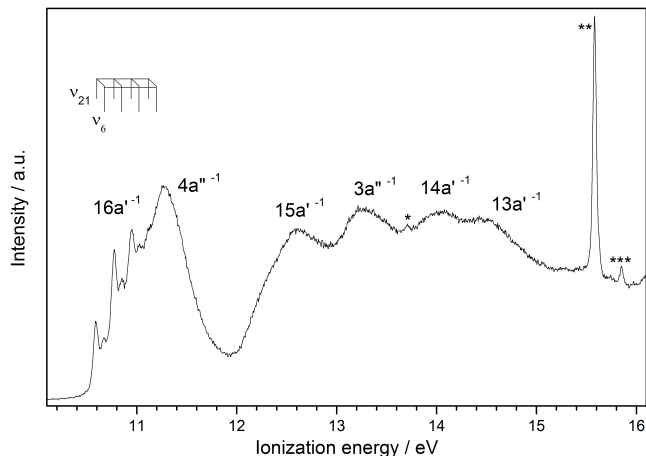
Figure 2. He(I) photoelectron spectrum of ethyl formate, $C_3H_6O_2$, in the 10.1–16.1 eV region (*N_2^+ $X^2\Sigma_g^+$, v' = 0 produced by the He_β line; **N_2^+ $X^2\Sigma_g^+$, v' = 0 produced by the He_α line; ***$N_2^+A^2\Pi_u$, v' = 1 produced by the He_α line) and assignment of the IEs.

adiabatic IE was evaluated using the optimized geometries of the neutral and ionic ground states. Additionally, the first and second ionization energies were calculated with the coupled-cluster singles and doubles (CCSD), and the coupled-cluster singles, doubles and perturbative triples (CCSD(T)) methods, employing the optimized geometries at the MP2/aug-cc-pVTZ level of approximation. The first IE of the s-cis,trans conformer of ethyl formate was also calculated at the MP2, CCSD and CCSD(T) levels using the aug-cc-pVQZ basis set in order to estimate the basis set effect. Furthermore, the zero point vibrational energy (ZPVE) corrections to the relative energies of the conformers and to the adiabatic IE's were determined from the MP2/aug-cc-pVTZ harmonic vibrational frequencies. These corrections were also applied to the values calculated with the CCSD and CCSD(T) methods. Higher IE's were obtained with the Partial Third Order (P3) propagator method using the aug-cc-pVTZ basis set and the MP2/aug-cc-pVTZ geometry. The Franck-Condon (FC) factors, associated to the first and second photoelectron bands of ethyl formate, were calculated using recursive relations and include Duschinsky rotation effects[22–24]. These calculations made use of the ground state geometries, harmonic frequencies and normal coordinates calculated with the MP2/aug-cc-pVTZ method for the neutral (S_0 state) and ionic (D_0 state) forms of ethyl formate. Next, the vertical excitation energies, oscillator strengths (f_L, in the length gauge) and electronic radial spatial extents ($< r^2 >$) of $s-cis,trans$ ethyl formate were calculated with the equation of motion coupled cluster method restricted to single and double excitations (EOM-CCSD) using the MP2/aug-cc-pVTZ geometry. Although the calculations have been made only for the more abundant conformer, the authors expect the the changes in excited

state energies between the conformers to be smaller that the intrinsic errors in calculations. To provide a better description of the Rydberg states, a set of diffuse functions (6s, 6p, 4d), taken from Kaufmann et al.[25] and localized on the central oxygen atom (O1), was added to the aug-cc-pVDZ basis set (named aug-cc-pVDZ + R). The electronic radial spatial extents of the states were calculated in order to help in the assignment of Rydberg states, which show comparable r^2 value for a given nl configuration. EOM-CCSD calculations were performed using the MOLPRO program[26].

IV. STRUCTURE AND PROPERTIES OF ETHYL FORMATE

In ethyl formate, $C_3H_6O_2$ there are two internal rotations that give rise to conformational isomerism[8]. The rotation around the (O=C−O) bond generates the s-cis and s-trans conformers, whereas the rotation about the O−R (R is the ethyl group) gives another two conformers: trans and gauche. From there, four stable conformations of ethyl formate can be obtained, s-cis, trans, s-cis,gauche, s-trans, trans and s-trans,gauche.

It has been shown that at room temperature (RT) both in the liquid and gas phase only two conformers are present, s-cis, trans, s-cis,gauche[7], with s-cis, trans being more stable[8]. Both configurations are shown in Fig. 3 and the relative energies of both conformers, calculated using MP2 geometries, are summarized in Table I. From the relative energies it can be seen that both conformers are present at RT with estimated populations of about 60 % for s-cis,trans and about 40 % for s-cis,gauche. The calculated spectroscopic properties of both conformers show many similarities. Therefore, in order to clarify the results presented here, only the results of s-cis,trans are described in the paper, whereas for the results on s-cis,gauche conformer see Supplementary Material Document No._ [27].

The s-cis,trans ethyl formate has C_s symmetry and its 27 normal coordinates separate in 17 vibrations of A' symmetry and 10 modes of A'' symmetry. Furthermore, the calculated electron configuration of the $\tilde{X}^1A'$ ground state is as follows: (a) core orbitals $(1a')^2$ $(2a')^2$ $(3a')^2$ $(4a')^2$ $(5a')^2$, (b) valence orbitals $(6a')^2$ $(7a')^2$ $(8a')^2$ $(9a')^2$ $(10a')^2$ $(11a')^2$ $(1a'')^2$ $(12a')^2$ $(2a'')^2$ $(13a')^2$ $(14a')^2$ $(15a')^2$ $(3a'')^2$ $(4a'')^2$ $(16a')^2$. The highest occupied molecular orbital (HOMO, 16a') in the neutral ground state is localized predominantly on the oxygen in-plane lone pair (n_O). The second highest occupied molecular orbital (HOMO-1, 4a'') corresponds mostly to the bonding π(C=O). The orbital 15a' (HOMO-3) shows a main contribution on the oxygen (O1) in-plane lone pair. The lowest unoccupied molecular orbital is mainly of π^* antibonding character and it is localized on the C=O bond.
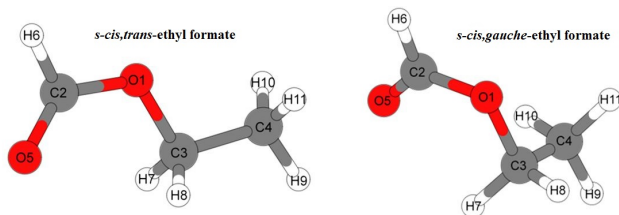
Figure 3. Structure of the two most stable conformers of ethyl formate: $s-cis,trans$ and $s-cis,gauche$.

Table I. Relative energies of the two most stable conformers of ethyl formate calculated using aug-cc-pVTZ basis set without and with inclusion of zero-point vibrational energies. The Boltzmann factors (in %), calculated at RT, are given in brackets.

ΔE / kcal mol^{-1}	$s-cis,trans$	$s-cis,gauche$
MP2	0.0 (52)	0.05 (48)
MP2+ZPVE	0.0 (58)	0.20 (42)
CCSD+ZPVE	0.0 (65)	0.36 (35)
CCSD(T)+ZPVE	0.0 (59)	0.21 (41)

V. RESULTS AND DISCUSSION

A. He(I) photoelectron

The He(I) photoelectron spectrum of ethyl formate, measured over the energy range of $10.0 - 16.1$ eV, is shown in Fig. 2. The calculated vertical and adiabatic IEs, obtained through various methods are shown in Table II for s-$cis,trans$ conformer. See Supplementary Material Document No. _ for the s-$cis,gauche$ calculated IEs[27]. In agreement with previous work[5] the IEs calculated with the MP2 method are overestimated in comparison to the experimental results. However, the lowest vertical (10.771 eV) and adiabatic (10.588 eV) IEs, observed in the photoelectron spectrum, agree reasonably well with the values obtained from calculations with the CCSD (10.903 eV and 10.491 eV, respectively) and CCSD(T) (10.988 eV and 10.605 eV, respectively). In particular, the CCSD(T) adiabatic value (10.605 eV), obtained with the large aug-cc-pVQZ basis set and including ZPVE correction, is in very good agreement with the experimental value (10.588 eV). Additionally, the calculated vertical IEs for $4a''^{-1}$ (11.435 eV with CCSD and 11.500 eV with CCSD(T)) are in reasonable agreement with the experimental values (11.227 eV and 11.28 eV[12]). The higher IEs calculated with the P3 methods allowed an assignment of the bands observed in the photoelectron spectrum (Fig. 2). Similar to what was found in our previous work on methyl formate[5], the P3 method has a tendency of overestimating the IEs of ethyl formate. This is particularly the case for the IEs $4a''^{-1}$ and $15a'^{-1}$, which present deviation with respect to experiment as large as 0.5 eV. Finally, the experimental values

obtained in our study are within reasonable agreement with the results of Benoit and Harrison[11] and Sweigart and Turner[12].
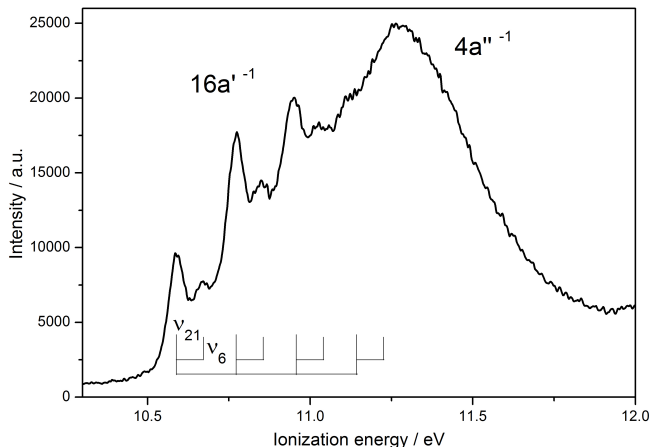

Figure 4. He(I) photoelectron spectrum of first two ionic states of ethyl formate with vibronic excitation assignment

The calculations presented in Table II show that the low energy part of the photoelectron spectrum with the resolved vibronic structure corresponds to the $16a'^{-1}$ ionic state (Fig. 4). The observed progressions can be classified into two groups, corresponding to separations of approximately 0.180 eV and 0.090 eV (Table III). In order to determine, which vibrational transitions are observed in the spectrum, calculations of frequencies together with Franck-Condon factors were performed, and are presented in Table IV and Fig. 5. According to the calculations, the first group of the more intense peaks, separated by ~0.180 eV, is mainly attributed to mode ν_{21}, which designates C$-$O and C=O stretches. The vibration ν_{16}, involving mostly CH$_2$ wagging, presents also a non-negligible contribution to this first group. The second group, separated by about 0.090 eV, is mostly ascribed to mode ν_6 that is O=C$-$O deformation with C$-$O stretch. In particular, the normal mode configuration may lead to Fermi resonances. Moreover, mode ν_7 provides an additional contribution to this second group of bands and involves C$-$O stretch and CH$_3$ rocking. Next, the band, centered at 11.227 eV, is assigned to $4a''^{-1}$ state (see Fig. 2 and Table II). This band does not exhibit vibrational structure and overlaps with the $16a'^{-1}$ band, although the nature of the features suggests that further modes and combinations may also contribute to the observed structure. Calculations of the FC factors for this state show that the lack of vibrational structure is due to overlapping peaks resulting from various combinations of vibrations (see Fig. 5).
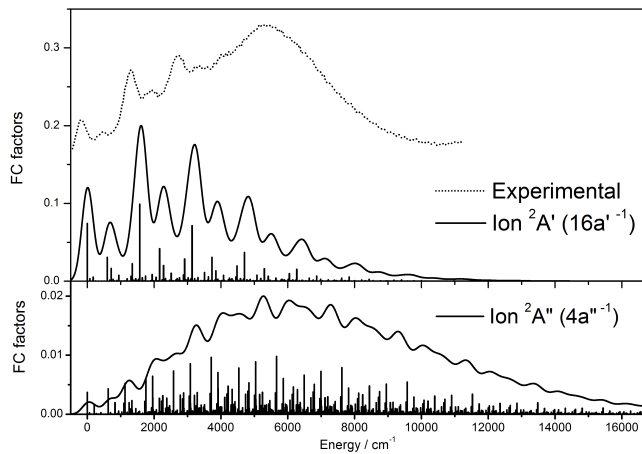
Figure 5. Comparison between experimental (dashed) and theoretical Franck-Condon (solid) vibrational structures of the first (upper, ion $^2A'(16a'^{-1})$) and second (lower, ion $^2A''(4a''^{-1})$) photoelectron bands of ethyl formate.

B. Valence states and transitions

The results of calculations presented in Table V allowed the assignment of absorption bands that are centered at 5.753, 7.465 and 8.292 eV to $(\pi^*(C=O)\leftarrow n_O, 16a')$, $(3s\sigma/\sigma^*(CH)\leftarrow n_O, 16a')$ and $(\pi^*(C=O)\leftarrow \pi(C=O), 4a'')$ transitions, respectively (Fig. 6, 7, 8). Pure Rydberg transitions of high oscillator strengths in this energy range are discussed later (see Section V C). Detailed assignment of the vibronic progressions that were found in these three bands is presented in Table VI.

The first band (Fig. 6) with a maximum absolute cross section of 0.217 Mb has been identified as the transition from the oxygen in-plane lone pair to the first π antibonding molecular orbital $(\pi^*(C=O)\leftarrow n_O, 16a')(1^1A''\leftarrow 1^1A')$. The calculated oscillator strength for this transition yields 1.43×10^{-3} and is comparable to the value obtained for methyl formate[5]. The associated vibronic series in this band, seen between 5.0 and 6.5 eV were attributed to CC stretching (ν_{13}), and assigned based on data of Maes et al.[8]. The broad nature of this band suggests that further modes, not resolved here, may be involved. The feature at 5.276 eV was tentatively assigned as the origin of this band.

A second absorption band (Fig. 7), centered at 7.465 eV with a maximum cross section of 11.603 Mb, was assigned to the $(3s\sigma/\sigma^*(CH)\leftarrow n_O, 16a')(2^1A'\leftarrow 1^1A')$ transition. The calculations indicate a mixed valence/Rydberg character ($3s\sigma$) for this state, nevertheless the high value of calculated oscillator strength (3.70×10^{-3}) is primarily due to valence ($\sigma^*(CH)$) character of this molecular orbital. The vibronic structure at 7.464 eV is proposed to be due mixed Rydberg/valence character, combined with two quanta of CH_3 rocking (ν_{12})[8], one quantum of combined CO stretch (ν_{21}) and one quantum of O=C−O deformation, coupled with C−O stretch (ν_6).

The third band, centered at 8.292 eV with a cross section of 21.469 Mb, was assigned to the $(\pi^*(C=O)\leftarrow \pi(C=O), 4a'')(3^1A'\leftarrow 1^1A')$ transition. The calculated oscillator strength for this transition has the highest value among all transitions identified in the spectrum, yielding 0.172, compared to methyl formate: 0.153.

Continued overlap of vibronic structures associated both with Rydberg and valence transitions is proposed for features above 7.9 eV (Fig. 7 and Fig. 8 together with Table VI). Due to a large number of bands (see Table V) in this region it was very difficult to assign transitions unambiguously.

C. Rydberg series

The photoabsorption spectrum above 7.4 eV shows a number of structures superimposed on a diffuse absorption feature extending to the lowest ionization energy. The proposed Rydberg transitions, that are labeled in Fig. 7 and Fig. 8 and presented in Table VII and Table VIII, originate mainly from the HOMO (16a') and HOMO-1 (4a'') according to computations. The positions of the peaks, E_n, have been tested using the Rydberg formula: $E_n = E_i - R/(n-\delta)^2$, where E_i is the ionization energy with adiabatic value of 10.588 eV, n is the principal quantum number of the Rydberg orbital of energy E_n, and δ is the quantum defect. Quantum defects are expected to be in range of 1.0–0.9, 0.6–0.3 and <0.25 for ns, np and nd series, respectively.

The feature at 7.465 eV was assigned to $(3s\sigma\leftarrow n_O, 16a')$ Rydberg transition with a quantum defect of 0.91 (Table VII) and is accompanied by vibronic structure for valence transition , discussed in Section V B. The higher members of this Rydberg series are proposed to extend to $n=6$. State $n=7$ was assigned purely on the value of the quantum defect.

The first members of $np\sigma$ $np\sigma'$ and $np\pi$ series were found at 8.046 eV, 8.222 eV and 8.382 eV with quantum defects of 0.69, 0.60 and 0.52, respectively (Table VII). Calculated energies for these transitions (Table V), yielding 8.333 eV, 8.524 eV and 8.675 eV agree with experimental values reasonably well, when the valence character of these transitions is accounted for. They are also associated with vibronic structure, as shown in Fig. 7. The higher members of this Rydberg series are proposed to extend to $n=6$ for the σ series, $n=4$ for the π series and $n=5$ for the σ' series. The feature at 8.774 eV was assigned to first transition of the $nd\sigma$, with $\delta=0.26$ and is also in a good agreement with the calculated value of 9.083 eV. For the $n=3$, the $nd\sigma$ and $nd\sigma'$ series show vibrational excitation with one quantum of combined CO stretch (ν_{21}) and one quantum of O=C−O deformation, coupled with C−O stretch (ν_6) each. The higher members of of these Rydberg series, of lowering relative intensity, are difficult to assign due to the overlap with other

transitions and vibronic structures.

Some tentative assignment of features belonging to other Rydberg series, which converge to the ionic electronic first excited state $\tilde{A}^2A''$ ($4a''^{-1}$) was performed (Figures 7 and 8 together with Table VIII). For the high energy members, the assignment was based purely on the values of the quantum defects.

D. Absolute photoabsorption cross sections and atmospheric photolysis

The photoabsorption cross sections presented in this work were measured for the first time for this compound. These absolute cross sections can be used in combination with solar actinic flux[29] measurements from the literature to estimate the photolysis rate of ethyl formate in the atmosphere from an altitude close to the ground to the stratopause at 50 km. Details of the programme are presented in a previous publication[30]. The quantum yield for dissociation following absorption is assumed to be unity. The reciprocal of the photolysis rate at a given altitude corresponds to the local photolysis lifetime. Photolysis lifetimes of less than 72 sunlit hours (6 days) were calculated at altitudes above 20 km. This indicates that ethyl formate molecules can be broken up quite efficiently by VUV absorption at these altitudes. While there is a fairly substantial photolysis rate at the higher altitudes leading to a correspondingly short lifetime of a few days or less, at lower altitudes the lack of solar actinic flux at the absorption wavelengths of this molecule lead to an extremely long lifetime (extending to months).

Rate constants for gas-phase reactions of OH radicals with ethyl formate have been studied and a value of $(5.66 \pm 1.10) \times 10^{-13} \exp[(134 \pm 53)/T]$ cm^{3}molecule^{-1}s^{-1} was measured in a temperature range of 233–372 K, such that these molecules may be transported further from their emission sources[31]. These results were confirmed later for ethyl formate oxidation in presence of chlorine atoms[32,33]. Calculated tropospheric lifetimes of ethyl formate reactions with OH have yielded a value of 13.6 days[31], which is still shorter than the photolysis lifetimes at the altitude of 19 km (16.4 days) and below (51 days at 18 km). This means that radical reactions must all be considered as the main loss processes for ethyl formate and UV photolysis is not expected to play a significant role in the tropospheric removal of these molecules.

VI. CONCLUSIONS

In this work we present for the first time complete electronic spectra of ethyl formate together with absolute photoabsorption cross sections from 4.5 to 10.9 eV. The structures that can be observed in the spectrum can be assigned to both valence and Rydberg transitions, based on ab initio calculations of vertical excitation energies and oscillator strengths of this molecule. Fine structure

has been assigned to vibrational series involving predominantly excitations of ν_{21} and ν_6 modes from C=O and C−O stretching. The high resolution He(I) photoelectron spectrum of ethyl formate has enabled vibrational excitations in the $\tilde{X}^2A'$($16a''^{-1}$) ionic electronic ground state of this molecule to be resolved and also assigned to ν_{21} and ν_6 modes. The theoretical calculations presented here are in a good agreement with experimental data, as well as in predicting a significant mixing of Rydberg and π^* states. Based on the photoabsorption cross section, photolysis lifetimes of ethyl formate have been calculated for the Earth's troposphere and stratosphere.

REFERENCES

[1] C. H. Bell, Crop Protection 19, 563 (2000).
[2] I. Medvedev, F. C. D. Lucia, and E. Herbst, The Astrophysical Journal Supplement Series 181, 433 (2009).
[3] I. Medvedev, F. C. D. Lucia, and E. Herbst, Astronomy and Astrophysics 499, 215 (2009).
[4] P. Osswald, U. Struckmeier, T. Kasper, K. Kohse-Hoeinghaus, J. Wang, T. A. Cool, N. Hansen, and P. R. Westmoreland, Journal of Physical Chemistry A 111, 4093 (2007).
[5] Y. Nunes, G. Martins, N. J. Mason, D. Duflot, S. V. Hoffmann, J. Delwiche, M.-J. Hubin-Franskin, and P. Limão-Vieira, Physical Chemistry Chemical Physics 12, 15734 (2010).
[6] J. M. Riveros and J. E. Bright Wilson, The Journal of Chemical Physics 46, 4605 (2010).
[7] S. W. Charles, G. I. L. Jones, N. L. Owen, S. J. Cyvin, and B. N. Cyvin, Journal of Molecular Structure 16, 225 (1973).
[8] I. I. Maes, W. Herrebout, and J. van der Veken, Journal of Raman Spectroscopy 25, 679 (1994).
[9] M. Chhiba, F. Tristram, and G. Vergoten, Journal of Molecular Structure 405, 113 (1997).

[10] D. van Raalte and A. G. Harris, Canadian Journal of Chemistry 41, 2054 (1963).

[11] F. M. Benoit and A. G. Harrison, Journal of American Chemical Society 99, 3980 (1977).

[12] D. A. Sweigart and D. W. Turner, Journal of American Chemical Society 94, 5592 (1972).

[13] M. Liu, C. Wu, Z. Wu, Q. Liang, Y. Deng, Q. Gong, Y. Sun, Y. Xu, Y. Zhao, X. Shan, F. Liu, and L. Sheng, Chemical Physics Letters 468, 153 (2009).

[14] S. Eden, P. Limão-Vieira, S. Hoffmann, and N. Mason, Chemical Physics 323, 313 (2006).

[15] N. Mason, J. Gingell, J. Davies, H. Zhao, I. Walker, and M. Siggel, Journal of Physics B-Atomic, Molecular and Optical Physics 29, 3075 (1996).

[16] W. Chan, G. Cooper, and C. Brion, Physical Review A 44, 186 (1991).

[17] J. Delwiche, P. Natalis, J. Momigny, and J. E. Collin, Journal of Electron Spectroscopy and Related Phenomena 1, 219 (1972-1973).

[18] K. Huber and C. Jungen, Journal of Chemical Physics 92, 850 (1990).

[19] D. Shaw, D. Holland, M. MacDonald, A. Hopkirk, M. Hayes, and S. McSweeney, Chemical Physics 166, 379 (1992).

[20] M. J. Frisch, G. W. Trucks, H. B. Schlegel, G. E. Scuseria, M. A. Robb, J. R. Cheeseman, G. Scalmani, V. Barone, B. Mennucci, G. A. Petersson, H. Nakatsuji, M. Caricato, X. Li, H. P. Hratchian, A. F. Izmaylov, J. Bloino, G. Zheng, J. L. Sonnenberg, M. Hada, M. Ehara, K. Toyota, R. Fukuda, J. Hasegawa, M. Ishida, T. Nakajima, Y. Honda, O. Kitao, H. Nakai, T. Vreven, J. A. Montgomery, Jr., J. E. Peralta, F. Ogliaro, M. Bearpark, J. J. Heyd, E. Brothers, K. N. Kudin, V. N. Staroverov, R. Kobayashi, J. Normand, K. Raghavachari, A. Rendell, J. C. Burant, S. S. Iyengar, J. Tomasi, M. Cossi, N. Rega, J. M. Millam, M. Klene, J. E. Knox, J. B. Cross, V. Bakken, C. Adamo, J. Jaramillo, R. Gomperts, R. E. Stratmann, O. Yazyev, A. J. Austin, R. Cammi, C. Pomelli, J. W. Ochterski, R. L. Martin, K. Morokuma, V. G. Zakrzewski, G. A. Voth, P. Salvador, J. J. Dannenberg, S. Dapprich, A. D. Daniels, . Farkas, J. B. Foresman, J. V. Ortiz, J. Cioslowski, and D. J. Fox, "Gaussian 09 Revision A.02," Gaussian Inc. Wallingford CT 2009.

[21] T. H. D. Jr., Journal of Chemical Physics 90, 1007 (1989).

[22] M. Łabuda and J. Guthmuller, European Physical Journal-Special Topics 222, 2257 (2013).

[23] J. Guthmuller, F. Zutterman, and B. Champagne, Journal of Chemical Theory and Computation 4, 2094 (2008).

[24] J. Guthmuller, F. Zutterman, and B. Champagne, Journal of Chemical Physics 131, 154302:1 (2009).

[25] K. Kaufmann, W. Baumeister, and M. Jungen, Journal of Physics B 22, 2223 (1989).

[26] H.-J. Werner, P. J. Knowles, G. Knizia, F. R. Manby, M. Schütz, P. Celani, T. Korona, R. Lindh, A. Mitrushenkov, G. Rauhut, K. R. Shamasundar, R. D. Adler, T. B.and Amos, A. Bernhardsson, A. Berning, D. L. Cooper, M. J. O. Deegan, A. J. Dobbyn, F. Eckert, E. Goll, C. Hampel, A. Hesselmann, G. Hetzer, T. Hrenar, G. Jansen, C. Koppl, Y. Liu, A. W. Lloyd, R. A. Mata, A. J. May, S. McNicholas, W. Meyer, M. E. Mura, A. Nicklass, D. P. O'Neill, P. Palmieri, D. Peng, K. Pfluger, R. Pitzer, M. Reiher, T. Shiozaki, H. Stoll, A. J. Stone, R. Tarroni, T. Thorsteinsson, and M. Wang, "Molpro, version 2010.1, a package of ab initio programs," (2012), http://www.molpro.net.

[27] "See supplementary material document no._ . for information on supplementary material, see http://www.aip.org/pubservs/epaps.htm,".

[28] P. Sinha, S. E. Boesch, C. Gu, R. A. Wheeler, and A. K. Wilson, The Journal of Physical Chemistry A 108, 9213 (2004).

[29] W. B. DeMore, S. P. Sander, D. M. Golden, R. F. Hampson, M. J. Kurylo, C. J. Howard, A. R. Ravishankara, C. E. Kolb, and M. J. Molina, "Chemical kinetics and photochemical data for use in stratospheric modeling, evaluation number 12, january 15," (1997).

[30] P. Limão-Vieira, S. Eden, P. Kendall, N. Mason, and S. Hoffmann, Chemical Physics Letters 364, 535 (2002).

[31] S. LeCalve, G. LeBras, and A. Mellouki, Journal of Physical Chemistry A 101, 5489 (1997).

[32] T. J. Wallington, M. D. Hurley, and A. Haryanto, Chemical Physics Letters 432, 57 (2006).

[33] J. J. Orlando and G. S. Tyndall, International Journal of Chemical Kinetics 42, 397 (2010).

Table II. Calculated vertical/adiabatic ionization energies (in eV) of ethyl formate (*s-cis,trans*) at the MP2/aug-cc-pVTZ geometry, compared with experimental values.

| Configuration | Calculated | | | | Experimental | | |
	P3	MP2	CCSD	CCSD(T)	This work	Benoit and Harrison[11]	Sweigart and Turner[12]
$^2A'$ $(16a'^{-1})$	11.162	11.327 / 10.890	10.847 / 10.432	10.927 / 10.540	10.771 / 10.588	10.61	10.96 / 10.62
	–	11.396 / 10.962[a]	10.903 / 10.491[a]	10.988 / 10.605[a]	–	–	–
$^2A''$ $(4a''^{-1})$	11.640	12.445 / 11.992	11.435	11.500	11.227	–	11.28
$^2A'$ $(15a'^{-1})$	13.082	–	–	–	12.582	–	–
$^2A''$ $(3a''^{-1})$	13.273	–	–	–	13.255	–	–
$^2A'$ $(14a'^{-1})$	14.099	–	–	–	13.947	–	–
$^2A'$ $(13a'^{-1})$	14.529	–	–	–	14.535	–	–
$^2A''$ $(2a''^{-1})$	14.954	–	–	–	–	–	–
$^2A'$ $(12a'^{-1})$	16.735	–	–	–	–	–	–
$^2A''$ $(1a''^{-1})$	17.050	–	–	–	–	–	–
$^2A'$ $(11a'^{-1})$	18.124	–	–	–	–	–	–

[a]Ionization energies calculated with the aug-cc-pVQZ basis set using the MP2/aug-cc-pVTZ geometry.

Table III. Energy positions and vibrational analysis of features observed in the first photoelectron band $(16a'^{-1})$ of ethyl formate.

Peak energy / eV	Assignment	ΔE (ν_{21}) / eV	ΔE (ν_6) / eV
10.588	Adiabatic IE	–	–
10.672	$1\nu_6$	–	0.089
10.771	$1\nu_{21}$	0.183	–
10.860	$1\nu_{21} + \nu_6$	–	0.089
10.950	$2\nu_{21}$	0.179	–
11.043	$2\nu_{21} + \nu_6$	–	0.093
11.129	$3\nu_{21}$	0.179	–

Table IV. Main vibrational transitions and Franck-Condon factors participating to the vibrational structure of the first photoelectron band for the *s-cis,trans* conformer of ethyl formate (MP2/aug-cc-pVTZ).

Vibrational state	Frequency[a]/ cm^{-1}	FC factor
0–0 (adiabatic)	0	0.0742
ν_6 (O=C−O deformation, C−O stretch)	596.1	0.0307
ν_7 (C−O stretch, CH3 rocking)	713.4	0.0163
ν_{16} (CH$_2$ wagging)	1344.6	0.0225
ν_{21} (C−O stretch, C=O stretch)	1567.5	0.0991
$\nu_{21} + \nu_6$	2163.6	0.0418
$\nu_{21} + \nu_7$	2280.9	0.02
$\nu_{21} + \nu_{16}$	2912.1	0.0286
$2\nu_{21}$	3135	0.0715
$2\nu_{21} + \nu_6$	3731	0.0306
$2\nu_{21} + \nu_7$	3848.4	0.0133
$2\nu_{21} + \nu_{16}$	4479.6	0.0196
$3\nu_{21}$	4702.5	0.0368
$3\nu_{21} + \nu_6$	5298.5	0.016
$3\nu_{21} + \nu_7$	5415.8	0.0063
$3\nu_{21} + \nu_{16}$	6047	0.0096
$4\nu_{21}$	6270	0.0152

[a]The MP2 vibrational frequencies were corrected by a scaling factor of 0.96[28].

Table V. Calculated vertical excitation energies (EOM-CCSD/aug-cc-pVDZ) (in eV) and oscillator strengths compared with the present experimental vertical energies and VUV absorption cross sections of $s-cis,trans$ ethyl formate; numbers in brackets indicate shoulder peak.

| State	E / eV	f_L	$\langle r^2 \rangle$	Main character	E_{exp} / eV	Cross section / Mb
^{1}A"	5.875	0.00143	69	16 a'→LUMO	5.753	0.22
^{1}A'	7.755	0.00370	110	16 a"→ 3s σ/σ*(CH)	7.465	11.60
^{1}A'	8.129	0.17179	82	4 a"→ LUMO	8.292	21.47
^{1}A"	8.221	0.00451	105	4 a"→ 3s σ/σ*(CH)	8.114	20.02
^{1}A'	8.333	0.06113	119	16 a'→3p σ/σ*(CH$_3$)	8.046	19.76
^{1}A"	8.524	0.00246	128	16 a'→ 3p π	8.222	21.28
^{1}A'	8.675	0.00693	137	16 a'→ 3p σ'/σ'*(CH)	8.383	19.72
^{1}A"	8.790	0.01273	123	4 a"→ 3p σ/σ*(CH$_3$)	8.707	21.45
^{1}A'	8.958	0.05008	126	4 a"→ 3p π	8.913	25.69
^{1}A'	9.083	0.02393	148	16 a'→ 3d σ/σ*	8.77(4)	23.26
^{1}A"	9.120	0.02713	141	4 a"→ 3p σ'/σ'*(CH)	9.030	24.18
^{1}A"	9.149	0.00042	76	15 a' → LUMO		
^{1}A"	9.326	0.00005	184	16 a'→ 3d π		
^{1}A"	9.351	0.00011	132	4 a"→ 3d σ	9.386	18.97
^{1}A'	9.354	0.00415	224	16 a'→ 3d σ'	9.037	23.99
^{1}A'	9.382	0.00229	201	16 a'→ 3d σ''		
^{1}A"	9.458	0.00015	214	16 a'→ 3d π'		
^{1}A'	9.512	0.00628	297	16 a'→ 4s σ	9.16(3)	19.67
^{1}A'	9.639	0.01165	359	16 a'→4p σ	9.336	18.75
^{1}A"	9.678	0.00070	384	16 a'→ 4p π	9.407	19.62
^{1}A'	9.712	0.01146	274	16 a'→ 4p σ'	9.443	21.59
^{1}A'	9.732	0.00265	229	4 a"→ 3d π		
^{1}A"	9.749	0.00034	197	4 a"→ 3d σ'	9.694	30.14
^{1}A'	9.772	0.00101	196	15 a' → 3s σ		
^{1}A"	9.819	0.00063	193	4 a"→ 3d σ''		
^{1}A'	9.844	0.01363	400	16 a'→ 4d σ		
^{1}A'	9.895	0.00043	213	4 a"→ 3d π'		
^{1}A"	9.968	0.00319	221	4 a"→ 4s σ	9.793	33.05
^{1}A"	9.986	<0.00001	566	16 a'→ 4d π		
^{1}A'	9.991	0.00244	626	16 a' → 4d σ'	9.709	30.13
^{1}A"	10.005	0.00160	269	4 a"→ 4p σ	9.967	36.54
^{1}A'	10.006	0.00112	609	16 a'→ 4d σ''		
^{1}A'	10.036	0.00027	631	16 a'→ 4d π'		
^{1}A'	10.063	0.00279	783	16 a'→ 5s σ	9.755	30.59
^{1}A"	10.109	0.02326	281	4 a" → 4p σ'	10.07(1)	38.71
^{1}A'	10.113	0.00131	909	16 a'→ 5p σ	9.861	34.23
^{1}A"	10.134	0.00021	993	16 a'→ 5p π		
^{1}A'	10.135	0.01303	385	4 a"→ 4p π	10.047	38.89
^{1}A'	10.158	0.00457	939	16 a'→ 5p σ'	9.91(1)	35.153
^{1}A'	10.188	0.01538	811	16 a'→ 5d σ		
^{1}A"	10.201	0.00001	340	4 a" → 4d σ		
^{1}A"	10.242	<0.00001	398	4 a"→ 4d σ'	10.341	40.82
^{1}A'	10.258	0.01479	185	15a'→ 3p σ		
^{1}A'	10.290	0.00325	1463	16 a'→ 5d σ'		
^{1}A'	10.342	0.00014	1347	16 a'→ 5d σ''		
^{1}A"	10.348	0.00003	939	16 a'→ 5d π		
^{1}A'	10.360	0.00296	1412	16 a'→ 6s σ	10.055	38.77
^{1}A"	10.370	0.00047	1519	16 a'→ 5d π'		
^{1}A'	10.372	0.00318	1253	16 a'→ 6p σ		
^{1}A"	10.393	0.02606	526	15 a'→ 3p π		
^{1}A"	10.413	0.00628	726	16 a'→ 6p π		
^{1}A'	10.414	0.00092	1616	16 a'→ 6p σ'		
^{1}A'	10.427	0.01369	520	4 a"→ 4d π		
^{1}A"	10.452	0.00588	472	4 a"→ 4d σ''		
^{1}A'	10.463	0.00467	1395	16 a'→ 6d σ		
^{1}A"	10.468	0.00005	532	4 a"→ 5s σ	10.428	40.90
^{1}A'	10.480	0.00914	1635	16 a'→ 6d σ'		
^{1}A"	10.500	<0.00001	583	4 a"→ 5p σ'	10.543	41.27
^{1}A"	10.538	0.00052	753	4 a"→ 5p σ	10.480	40.99
^{1}A"	10.609	0.00370	924	4 a"→ 5p π		
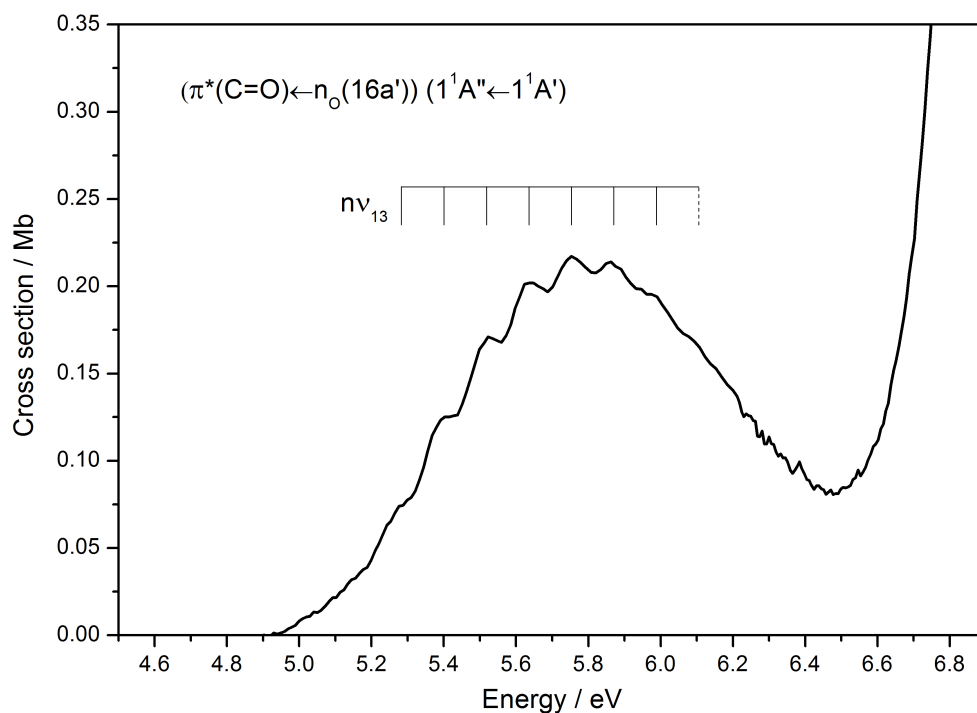
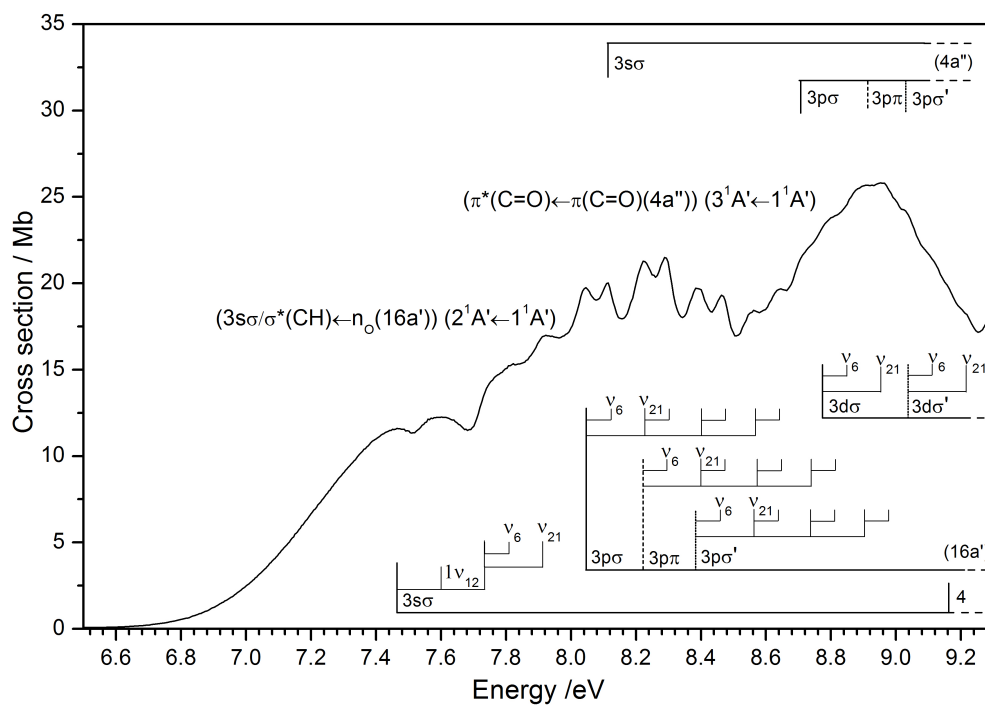Figure 6. Vibrational progressions in the 4.5–6.9 eV absorption band of ethyl formate, $C_3H_6O_2$.

Figure 7. Vibrational progressions and Rydberg series assignment in the 6.5–9.3 eV absorption band of ethyl formate, $C_3H_6O_2$.
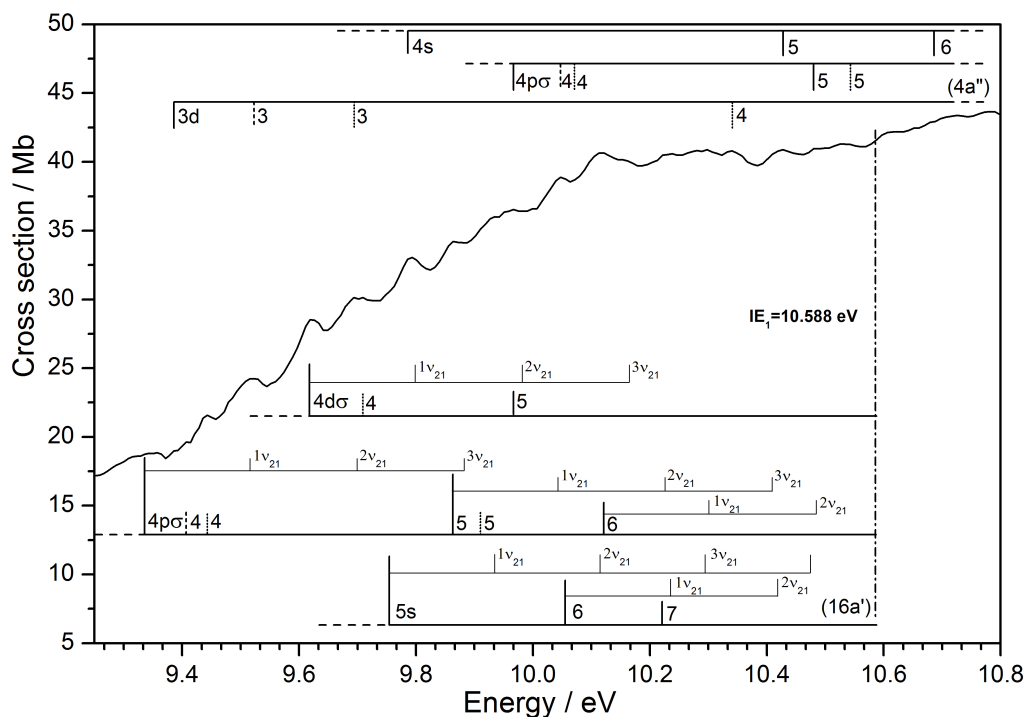
Figure 8. Vibrational progressions and Rydberg series assignment in the 9.25–10.8 eV absorption band of ethyl formate, $C_3H_6O_2$.

Table VI. Proposed vibrational assignments in the 5.0–9.2 eV absorption bands of ethyl formate, $C_3H_6O_2$.

Energy/eV	Assignment	$\Delta E(v'_6)$/eV	$\Delta E(v'_{12})$/eV	$\Delta E(v'_{13})$/eV	$\Delta E(v'_{21})$/eV
First band: $\pi^*(C{=}O)\leftarrow n_O(16a')$					
5.276	v_{00}	–	–	–	–
5.402	$1v_{13}$	–	–	0.126	–
5.523	$2v_{13}$	–	–	0.121	–
5.636	$3v_{13}$	–	–	0.113	–
5.753(v)[a]	$4v_{13}$	–	–	0.117	–
5.862	$5v_{13}$	–	–	0.109	–
5.975	$6v_{13}$	–	–	0.113	–
6.093	$7v_{13}$	–	–	0.118	–
Second band: $3s\sigma/\sigma^*\leftarrow n_O(16a')$					
7.464	v_{00}	–	–	–	–
7.602	$1v_{12}$	–	0.138	–	–
7.744	$2v_{12}$	–	0.142	–	–
7.815	$2v_{12}+1v_6$	0.071	–	–	–
7.920	$2v_{12}+1v_{21}$	–	–	–	0.176
Third band: $\pi^*(C{=}O)\leftarrow n_O(4a'')$					
8.046	v_{00}	–	–	–	–
8.114	$v_{00}+1v_6$	0.068	–	–	–
8.223	$1v_{21}$	–	–	–	0.177
8.288	$1v_{21}+1v_6$	0.065	–	–	–
8.389	$2v_{21}$	–	–	–	0.166
8.463	$2v_{21}+1v_6$	0.074	–	–	–
8.557	$3v_{21}$	–	–	–	0.168
8.640	$3v_{21}+1v_6$	0.083	–	–	–

[a] (v) is a vertical value

Table VII. Energies (in eV), quantum defects and assignments of the ns, np and nd Rydberg series converging to the $\tilde{X}^2A'(16a'^{-1})$ ionic electronic ground state of ethyl formate

Vertical transition energy	Quantum defect, δ	Assignment
7.464	0.91	$3s\sigma$
9.163	0.91	$4s\sigma$
9.755	0.95	$5s\sigma$
9.935	–	$5s\sigma+1\nu_{21}$
10.055	0.95	$6s\sigma$
10.221	0.91	$7s\sigma$
10.115	–	$5s\sigma+2\nu_{21}$
10.295	–	$5s\sigma+3\nu_{21}$
8.046	0.69	$3p\sigma$
9.336	0.70	$4p\sigma$
9.863	0.67	$5p\sigma$
10.113	0.65	$6p\sigma$
10.165	–	$4d\sigma+3\nu_{21}$
8.222	0.60	$3p\pi$
9.407	0.61	$4p\pi$
8.383	0.52	$3p\sigma'$
9.443	0.55	$4p\sigma'$
9.910	0.52	$5p\sigma$
8.774	0.26	$3d\sigma$
9.619	0.25	$4d\sigma$
9.967	0.32	$5d\sigma$
9.037	0.04	$3d\sigma'$
9.709	0.07	$4d\sigma'$

Table VIII. Energies (in eV), quantum defects and assignments of the ns, np and nd Rydberg series converging to the $\tilde{A}^2A''(4a''^{-1})$ ionic electronic first excited state of ethyl formate

Vertical transition energy	Quantum defect, δ	Assignment
8.114	0.91	3sσ
9.786	0.93	4sσ
10.428	0.87	5sσ
10.686	0.98	6sσ
8.707	0.68	3pσ
9.967	0.71	4pσ
10.480	0.73	5pσ
8.913	0.58	3pπ
10.047	0.60	4pπ
9.030	0.51	3pσ'
10.071	0.57	4pσ'
10.543	0.54	5pσ'
9.386	0.28	3dσ
10.298	0.17	4dσ
9.694	0.02	3dσ'
10.341	0.08	4dσ'
9.523	0.17	3dπ
10.280	0.21	4dπ